UNIVERSITY OF GRONINGEN

The Blaauw Spectrograph design

Author:
M. LENSEN (S2975947)

Supervisor:
DR. J. NOEL-STORR

July 25, 2021

1 Project description

This report describes the design of an Integral Field Spectrograph (IFS) for the 40cm Gratama telescope in the Blaauw observatory. The spectrograph is to be used for astronomy students of The University of Groningen as part of their observational courses and for possible bachelor/master projects to get acquainted with modern-day astronomical observation techniques. Since the foundation of this project was laid years ago, we will build upon this. This mainly concerns using the IFU-head, fibers and grating which are already in possession. My involvement in the project covers the design of the optical model and building the optical parts of the spectrograph. Moreover, together with Daan Vermaat, I am involved in the mechanical design of components needed for the spectrograph. Other possible commitments are helping with practicalities concerning fiber infrastructure, aligning, polishing and project management. Finally, we have weekly meetings to discuss progress on the optics and mechanical parts with prof. dr. Marc Verheyen, dr. Jacob Noel-Storr, Rik ter Horst and Daan Vermaat.

Contents

2 Introduction

For some decades Integral Fields Spectroscopy (IFS) has allowed astronomers to combine spectrographic and imaging methods to obtain information about extended objects in a relatively short amount of time. By using an array of collecting elements and feeding the signal of each element into a spectrograph, a (1 dimensional) spectrum is generated for each individual element. Since the spatial (2 dimensional) position of each element on the sky is also known, these 3 dimensions can be combined into a data-cube. An example of what such a data-cube looks like can be found in Figure 1.

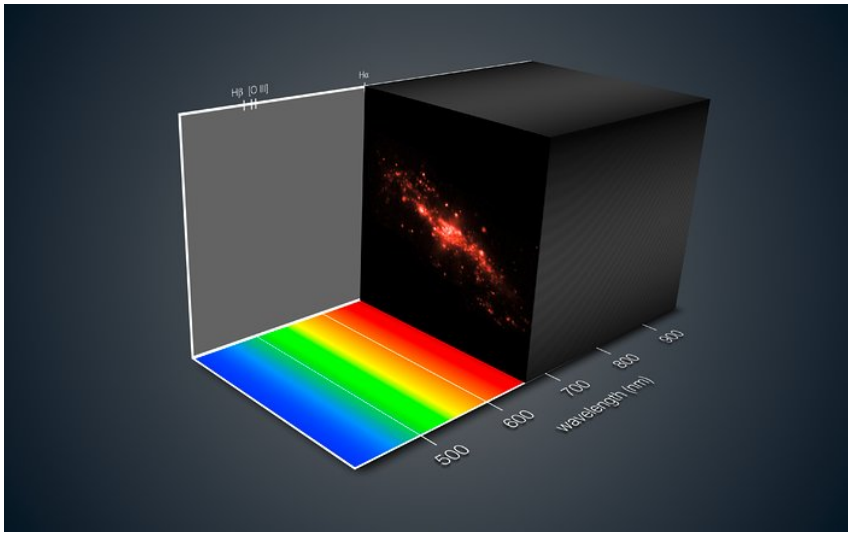

Figure 1: Data-cube of the galaxy NGC 4650A Source: ESO, retrieved on 23-04-2021.

There are various types of Integral Field Units (IFUs) used for imaging spectroscopy such as microlens arrays, image slicers or optical-fiber bundles. For our spectrograph, we will make use of the latter, optical fiber bundles. A general overview of how this works can be found in Figure 2. In section 4, a more detailed and specific description for our case is given.

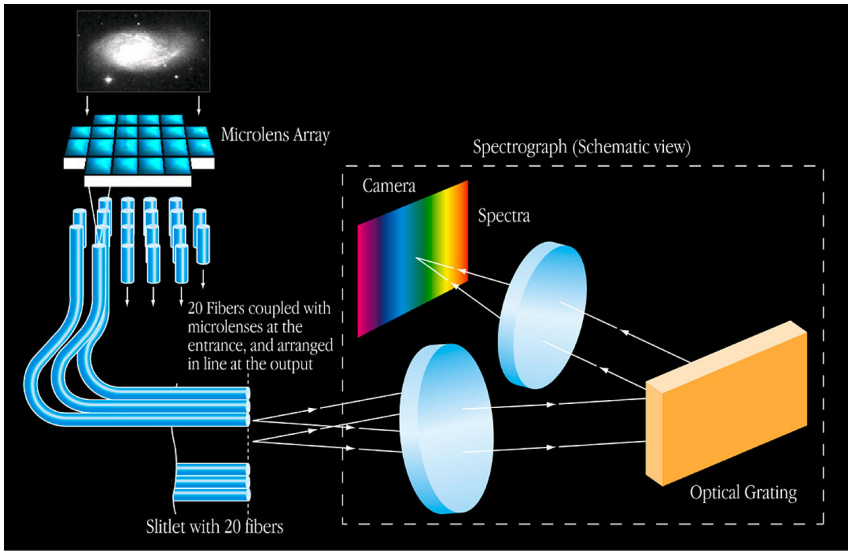

Figure 2: Schematic overview showing the principle of a fiber-based IFU. Source: ESO, retrieved on 23-04-2021.

For our design, we do not have definite requirements set on the spectrograph in terms of spectral resolution and coverage. However we would like to resolve certain interesting emission and absorption lines such as H_α (656 [nm]), H_β (486 [nm]) and O[III] (501 [nm] and 496 [nm]). We would like to aim for a spectral coverage of 400 to 700 [nm] and spectral resolution better than 1 [nm]. A larger spectral coverage than stated could mean that diffracted orders show overlap which would complicate things as described in Section 3.3.2. Moreover, to save time and money we will use the existing components.

Requirements set on the spectrograph by using the components available are summarized by:

- A spectral coverage of 400 to 700 [nm]
- spectral resolution $d\lambda < 1$ [nm]
- Make optimal use of the full-frame 24 [mm] x 36 [mm] CCD camera's chip
- Make use of the grating available
- Make use of the fibers available

A detailed description of the available components (detector, grating and fibers) can be found in Section 3.

Using these requirements, the goal is to create one functional optical design for the spectrograph. Geometrical calculations using Python and dedicated optical design software (OpticStudio, originally called Zemax) will be used to obtain possible designs with their corresponding conditions. Based on the desired requirements and limitations of the components, this will then give a baseline design for the spectrograph. The aim is to build the spectrograph based on the baseline design and using the available and purchased components.

3 Theory and specifications

3.1 Optical fibers

Light from the telescope is focused into the IFU-head packed with optical fibers where the light is collected at the focal plane and transported to the spectrograph room. Our fibers are multi-mode silica fibers (Polymicro Technologies FBP200220240) with core/cladding/buffer diameters of 200/220/240 [μm] respectively. The IFU contains 75, 13 meter long fibers including science-fibers, calibration-fibers and spare-fibers. The fibers are said to have an ideal acceptance angle or numerical aperture (NA) of 0.22 where the definition of NA is given by Equation 1. [van Assen, 2011]

$$NA = \sqrt{n_{core}^2 - n_{clad}^2} \tag{1}$$

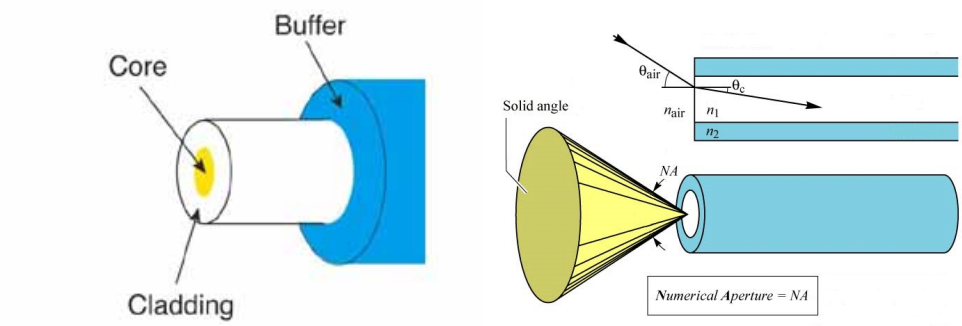

Figure 3: Left: Schematic diagram showing the optical fiber components. Source: FOA reference guide. Right: Diagram showing the cone acceptance angle of a optical fiber. Source: Gustavo Amaral, retrieved on 22-04-2021.

In an ideal situation, the light entering an optical fiber would come out in the same way. Due to many processes affecting the light in the fiber this is however not the case. The most important feature changing the output of the fiber is Focal Ratio Degradation (FRD). Since the Gratama telescope has a focal ratio f/8, this is the input for our fibers. Research done on our fibers used shows that for this input, the output focal ratio is f/5 (NA=0.1) for 80 $\%$ integrated light. Figure 4 shows what the integrated light intensity as function of output cone is. [van Assen, 2011] This profile will help us to set the optical model up and will give an estimate about what image each individual fiber will project on our detector.

3.2 IFU-head

In the focal-plane of the telescope, optical fibers are hexagonally packed into the IFU-head. The IFU-head is the collecting element of the spectrograph as explained above. Figure 5 shows a schematic diagram of what the IFU-head looks like, an hexagonal shaped cluster with 61 fibers and 6x2 additional sky-fibers for background subtraction.
The plate-scale of the Gratama telescope is equal to

$$p = \frac{206265\ arcsec}{f} = \frac{206265\ arcsec}{3200mm} = 64.5[arcsec\, mm^{-1}]. \tag{2}$$

Since the core of the optical fibers is 200 [μm], each fiber subtends 12.9 [arcsec] on the sky. The total span of the IFU is then (depending on orientation) approximately 135 [arcsec].

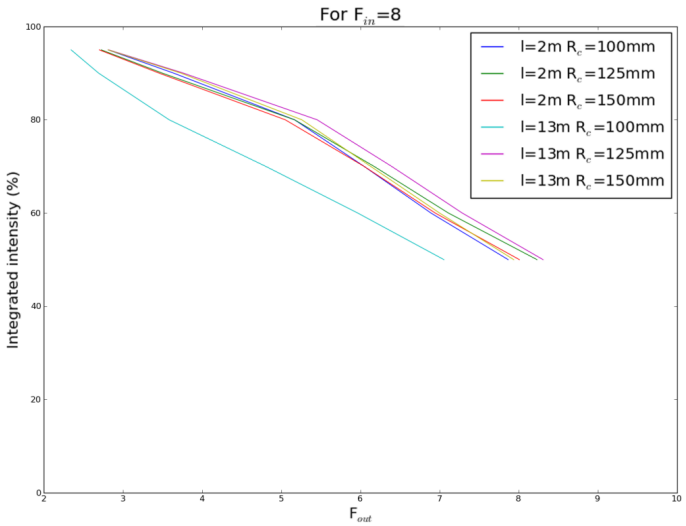

Figure 4: Integrated light intensity as function of output focal ratio and input focal ratio of f/8 (telescope) for various lengths and curvatures of the optical fibers. [van Assen, 2011]

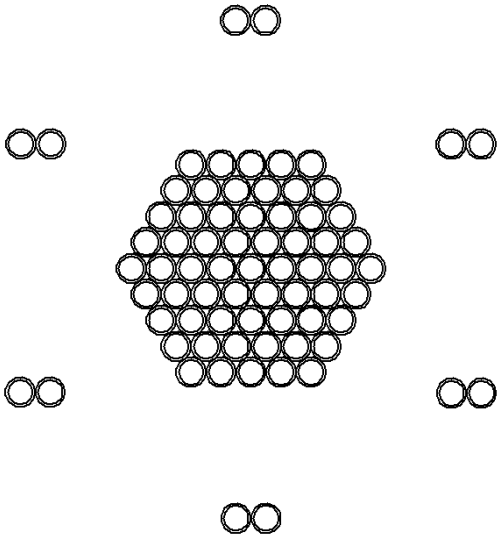

Figure 5: Drawing showing the hexagonally-shaped fiber cluster and 6x2 sky fibers showing the fiber mapping in the IFU-head.

As can be seen in Figure 5, there are gaps in between fibers due to the hexagonal structure and cladding/buffer of the optical fibers. The 'gap' between 2 fibers is 40 [μm] or about 2.5 [arcsec]. A hexagonal packing arrangement has a filling factor of 0.907 and taking into account the cladding and buffer, our filling factor is equal to $\rho = 0.907 \cdot \frac{r_{core}^2}{r_{buf}^2} = 0.907 \cdot \frac{200^2}{240^2} = 0.630$.

For optimal coupling efficiency of the light from the telescope into the fibers, the focused spot should be matched to the core size. In Groningen, a typical seeing-disk is about 2.5 [arcsec] which translates into a spot of about 40 [μm] for the Gratama telescope. This indicates that our fiber-cores are quite large compared with the optimal fiber-coupling.

3.3 Diffraction grating

For the diffracting element in our spectrograph we will make use of a diffraction grating. A diffraction grating is an element with periodic structures diffracting light and separating the light based on its wavelengths and can be transmissive or reflective.

The periodic structures can be of different shapes such as rectangular, sinusoidal, or triangular with different angles. A triangular grating is often used since this structure can easily be optimised for a certain wavelength (blaze-wavelength), this type of grating is also known as a blazed grating. The shape of the structure in general does not influence the dispersion angle and is only used for optimizing certain wavelengths and orders.

The functioning of a grating can be described by using Figure 6. Incoming collimated light (planar wave-front) hits the separated structures which act as individual slits. Following the Huygens-Fresnel principle, each slit then produces a spherical wave-front. At every point in space the diffracted light is the sum of all interfering spherical waves emanating from each individual slit. The interference is due to the optical path difference (OPD) between the slits to any point in space and is given by Equation 3

$$OPD = d(sin\theta_i + sin\theta_m) \tag{3}$$

Where θ_i is the angle of incidence w.r.t. the grating normal, θ_m is the angle of diffraction w.r.t. the grating normal and d the constant spacing between the slits.

Now when the OPD between two adjacent slits is equal to $m\lambda$ where m is an integer number and λ the wavelength of the light, the light coming from each slit constructively interferes and creates a maxima while for all other OPDs they do not, and the averaged light coming from all individual slits cancels out. This principle gives rise to the grating equation as given in Equation 4.

$$sin\theta_i + sin\theta_m = \frac{m\lambda}{d}, \tag{4}$$

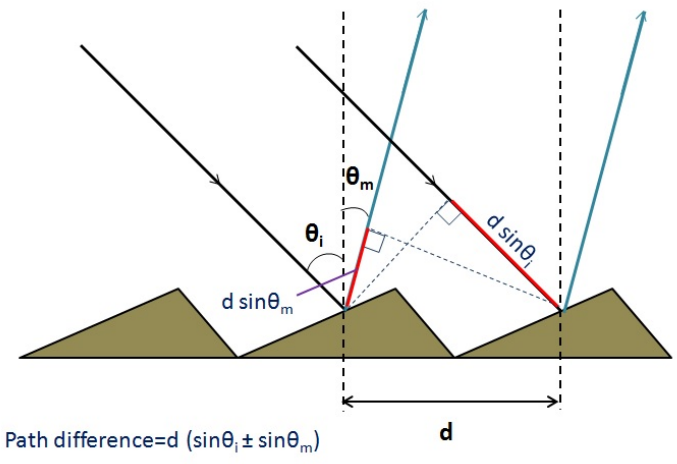

Figure 6: Diagram showing the path difference between incoming and outgoing rays due to the periodic structures on the reflection grating. Source: Wikipedia, retrieved on 22-04-2021.

The implication of this is that there are infinite orders (m) of maxima of the diffracted light (the diffraction pattern). The zeroth order will not show any diffraction because there is not path length difference

so that the diffraction grating will act like a mirror. An example of what such a diffraction pattern consisting of multiple order of diffracted light can be found in Figure 7.

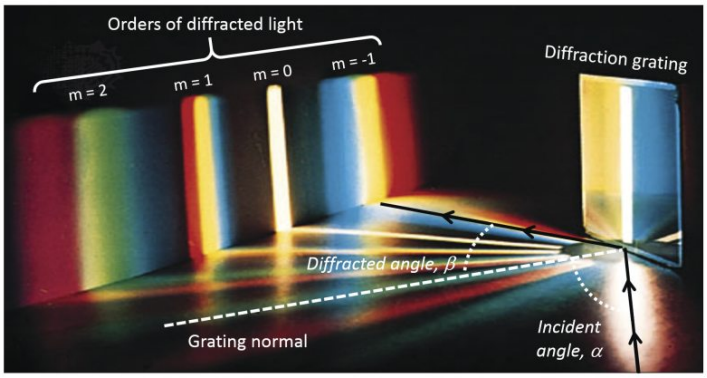

Figure 7: Image showing a diffraction grating and the different orders (m) of diffracted light. Source: Newport , retrieved on 23-04-2021.

As stated before, we already have a ruled reflection grating in possession. The grating is a Bausch and Lomb Nr 35-53-18-58 with the following specifications;

- Size 110 [mm] x 110 [mm]
- line spacing 2.5 [μm] (400[l/mm])
- blaze angle 9.773 [°]

3.3.1 Dispersion

As shown in the grating equation, we see that the angle of diffraction is dependent on wavelength of light. This implies that if collimated, polychromatic light falls onto the grating, every wavelength will be diffracted at a different angle creating a rainbow of light or angular dispersion as visible in Figure 7. From the grating equation it is also visible that there is more dispersion in higher orders and for smaller spacing's (more lines per millimeter).

When we differentiate the grating equation (where we have set $\theta_i = \alpha$ and $\theta_m = \beta$) w.r.t wavelength, we obtain the following relation;

$$\frac{d(sin\alpha + sin\beta)}{d\lambda} = \frac{d(m\lambda)}{d\lambda d}, \tag{5}$$

Which translates to;

$$\frac{dsin\beta}{d\lambda} = \frac{cos\beta d\beta}{d\lambda} = \frac{m}{d}, \tag{6}$$

So that we find;

$$\frac{d\beta}{d\lambda} = \frac{m}{dcos\beta}, \tag{7}$$

Which is the angular dispersion. If we collect the dispersed light using a lens with focal length f, the angular dispersion can be translated to a linear dispersion since $dx \approx fd\beta$, from which we find;

$$\frac{dx}{d\lambda} = \frac{m}{fdcos\beta} \tag{8}$$

3.3.2 Free spectral range

The free spectral range of a grating is maximum spectral bandwidth that can be obtained without overlap from light of adjacent orders. Figure 8 shows what this looks like, it is visible that the higher the order, the smaller the spectral bandwidth available. The free spectral range is given by;

$$FSR = \lambda_1 - \lambda_2 = \frac{\lambda_1}{m} \tag{9}$$

For our case we have $\lambda_1 = 400\ [nm]$, thus the free spectral range in the first order is 400 [nm], so that the full range from $\lambda_1 = 400\ [nm]$ to $\lambda_2 = 700\ [nm]$ can be covered. We also find that we can never cover the full range in the second order, this could however be solved by using filters to block adjacent orders.

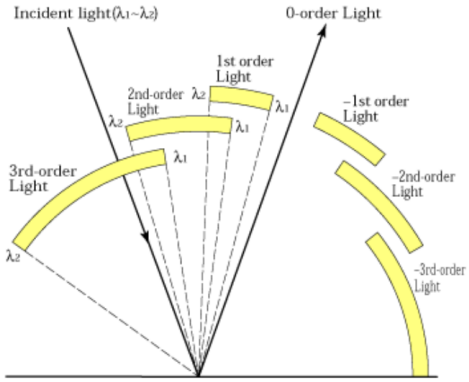

Figure 8: Image showing the diffraction of multiple orders of grating, indicating possible overlap for adjacent orders. Source: shimadzu, retrieved on 23-04-2021.

3.3.3 Anamorphic (de)magnification

Another effect which has to be taken into account when designing as spectrograph is the anamorphic magnification. The dispersed, collimated beam of light has changed in diameter due to projection effects of the grating. The beam can be either magnified of de-magnified depending of the angle of incidence and angle of diffraction as given in the following relation;

$$AM = \frac{cos(\beta)}{cos(\alpha)} \tag{10}$$

Due to this effect, having the grating tilted at relatively high angles w.r.t. the incoming beam might cause diffracted beam to become significantly large, possibly overfilling successive lenses. Figure 9 shows what the anamorphic effect looks like.

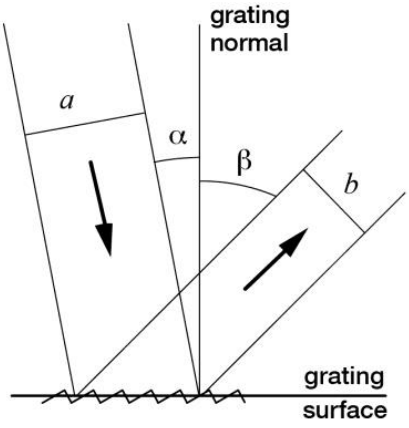

Figure 9: Diagram showing the princple of anamorphic magnification. Source: Christopher Palmer, retrieved on 25-04-2021.

3.3.4 Blaze wavelength

The blaze-angle of our grating is 9.773 [°], corresponding to θ_B in Figure 10. The blaze angle determines wavelength and order at which the interference signal is maximum by shifting the projected interference pattern.

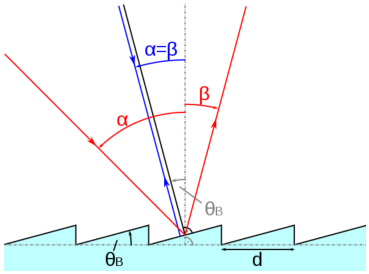

Figure 10: Figure showing the grating geometry. Source: Wikipedia, retrieved on 25-04-2021

We can determine at which angle of incidence and order we could work (to optimise throughput) using the following equation;

$$m\lambda_b = 2dsin(\gamma)cos(\alpha - \gamma) \tag{11}$$

Where γ is the blaze-angle (or θ_B). For our grating with spacing $d = 2.5[\mu m]$ and blaze angle $\gamma = 9.773[^\circ]$ we find;

$$m\lambda_b = 848.73 \cdot cos(\alpha - 9.773)[nm] \tag{12}$$

For the first order (m=1) Littrow configuration ($\alpha = \beta = \gamma$) we find that $\lambda_b = 849\ [nm]$. If we want to put the maximum intensity at our central wavelength (550 [nm] and for the first order) we have;

$$\alpha = arccos(\frac{550}{848.73}) + 9.773 = 59.3[^\circ] \tag{13}$$

This angle found is not feasible due to the enormous dispersion and resulting diameter of the beam entering the camera lens (L2). This also implies that the grating is not designed to be used in the optical regime in the first order. A possible solution to this might be that it could be used in the second order

(m=2). Using the second order and a angle of incidence α of 10 degrees will result in a blaze wavelength of about 425 [nm] which is quite good for optical wavelengths of 350 [nm] to 700 [nm] keeping in mind that the efficiency drops of more slowly for longer wavelengths than for shorter wavelengths. The typical efficiency curve for a 9 degree (similar to our 9.773 degree) blazed grating (in Littrow configuration) can be found in Figure 11. We estimate the efficiency at 400 [nm], when $\frac{m\lambda}{d} = \frac{1 \cdot 400}{2500} = 0.16$ to be 0.1 and at 700 [nm] to be 0.70 which will be used to determine the spectrographs throughput. The exact values (specifications) of our grating could unfortunately not be obtained.

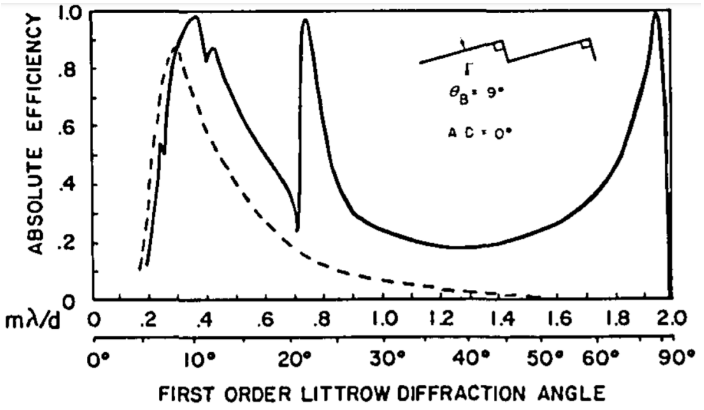

Figure 11: Figure showing the typical grating efficiency profile for a 9 degree blazed grating. Solid line is S-polarised and dashed line is P-polarised. Source: OSA publishing, retrieved on 05-05-2021.

3.4 Lenses

For our optical model and spectrograph we will make use of lenses to collimate light and focus it onto our detector. Various lenses were tested as described in Section 4.2.2 but eventually, based on the optical model, we decided that photographic lenses are needed to achieve high resolution. Based on desired specifications and availability we chose to go for the Canon EF 200mm f/2.8L II USM which we purchased. These lenses are said to have excellent optical quality (to be tested) and also show relatively high transmission in the UV. In Figure 12 the lens used is shown together with the transmission curve as obtained from literature [CAOS, 2021].

Figure 12: Left: Canon EF 200mm f/2.8L II USM photographic lens. Source:apollo, retrieved on 05-05-2021. Right: Transmission curve for Canon EF 200mm f/2.8L II USM photographic lens. Source: CAOS, retrieved on 05-05-2021.

3.5 Detector

As our detecting element, we will use a CCD camera since they offer low-noise and high quality images at low-light levels. We will make use of the SBIG STXL-11002 full-frame (36 [mm] x 24 [mm]) 11 Megapixel monochrome camera. The exact specifications of the detector can be found below [Diffraction-limited, 2021].

- Chip Size 36.0 [mm] x 24.7 [mm]
- Pixels; 4008 x 2672
- pixel size 9 [μm] x 9 [μm]

Another interesting parameter of the CCD is the quantum efficiency of the chip which will be used to estimate the spectrograph throughput. Figure 13 shows what the QE-profile of our detector looks like.

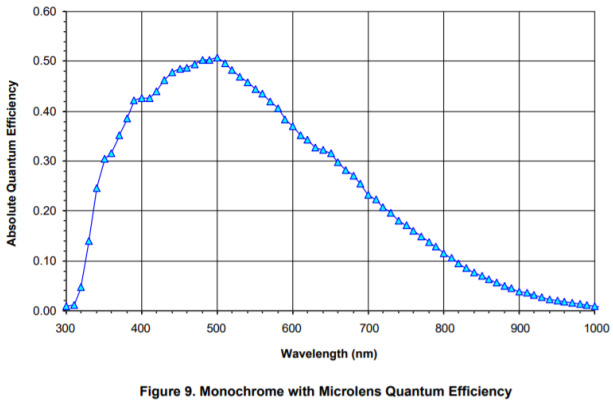

Figure 13: QE of kodak KAI-11002. Source: Kodak, retrieved on 25-04-2021.

4 Optical model

We would like to make an optical model of what the spectrograph should look like to see which lens- and parameter-configurations work. Using Zemax/Opticstudio we will investigate multiple models which will be substantiated using geometric calculations.

At first, light is collected by the telescope and focused in the focal plane. The focal plane consists of a bundle of 75 optical fibers forming the IFU-head where light is fed into the fibers and transported from the telescope to the (dark) spectrograph room. The 75 fibers are stacked on top of each other forming a pseudo-slit of $\sim$ 0.2 [mm] x 21 [mm]. The slit is then used as entrance aperture for the spectrograph. A simple overview of the working principle of our spectrograph can be found in Figure 14 where the 'telescope focal plane' should be replaced by the pseudo-slit.

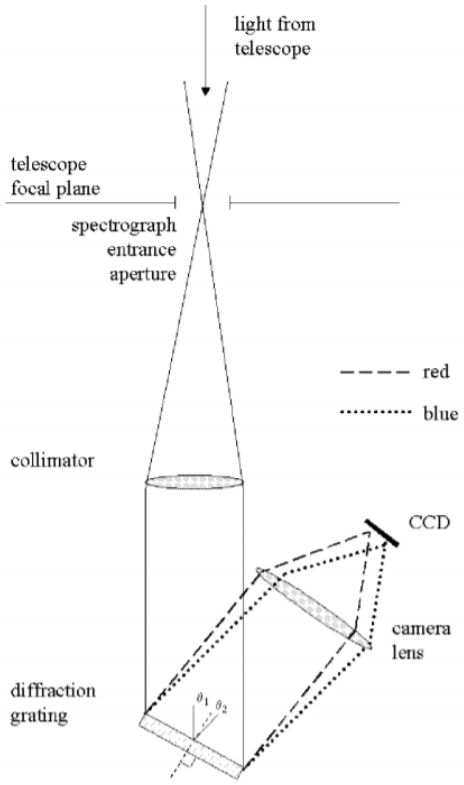

Figure 14: Schematic overview a grating spectrograph with a reflective grating. In this image, θ_2/β is larger than θ_1/α and the anamorphic magnification is larger than 1. Source: Sheila J. Kannappan, retrieved on 04-03-2021.

The light emitted by the fibers (f/5 - 80% integrated light for f/8 input [van Assen, 2011]) hits the first lens L1 with focal length f1 which is placed at a distance f1 from the fibers creating a collimated beam. The collimated beam then travels towards the reflection (diffraction) grating which disperses the light following the grating equation (equation 4). The light is dispersed light into all wavelengths which are emitted at different angles β, while maintaining collimation. The collimated beams are then collected by the second lens L2 with focal length f2 which focuses each wavelength (angle of incidence) onto a different point in the image plane at a distance f2 from lens L2. The 75 fibers in the slit-direction are then all imaged onto the CCD together with the spectra corresponding to each fiber in the dispersion-direction creating a 3D data-cube as described in Section 2.

4.1 Geometric paraxial model

Using the thin lens approximation, slit geometry, grating parameters, wavelength range and CCD dimensions we can set up our model and see which lens-configurations and geometries give the optimal (and desired) result.

We begin with the source (75 fibers pseudo-slit in our case) with a height y_0 of 21 [mm] and width $x_0 = 0.2[mm] \approx 0$. The light from each fiber exits the glass with an numerical aperture $\text{NA}_0 = 0.1$ or a maximum half-angle of $arcsin(0.1) \approx arctan(0.1) = 5.71°$. The height of the beam at L_1 (at distance f_1) is than given by

$$y_1 = y_0 + 2f_1 NA_0 = 21 + 0.2f_1[mm] \tag{14}$$

and the width by

$$x_1 = 0.2f_1[mm] \tag{15}$$

Now the collimated beams travels another distance f_1 to the grating G where the light is dispersed following the grating equation, Equation 4. We have;

$$sin(\beta) = \frac{m\lambda}{d} - sin(\alpha) \tag{16}$$

so that

$$\begin{aligned} \beta_{max} &= arcsin(\frac{m\lambda_{max}}{d} - sin(\alpha)) \\ \beta_c &= arcsin(\frac{m\lambda_c}{d} - sin(\alpha)) \\ \beta_{min} &= arcsin(\frac{m\lambda_{min}}{d} - sin(\alpha)) \end{aligned} \tag{17}$$

The total cone reflected by the grating is given by;

$$\Delta\beta = |\beta_{max} - \beta_{min}| \tag{18}$$

The outgoing, collimated, dispersed light than travels towards the second lens L2. The width of each collimated beam reflected by the grating is given by $x_{2,s} = \frac{cos(\beta)}{cos(\alpha)} \cdot x_1$ due to anamorphic magnification. This would correspond to a total width of $x_{2,t} = 2f_2 \cdot tan(\frac{\Delta\beta}{2}) + x_{2,s}$. The y-height is equal to $y_2 = y_1 \frac{f_2}{f_1}$.

Lens L2 is placed at an offset angle approximately β_c w.r.t. the grating normal. The light is focused by L2 on the image plane at a distance f2 from lens L2. The x-position in the image plane is given by

$$x_3 = 2 \cdot f_2 \cdot tan(\frac{\beta}{2}) \tag{19}$$

So that we find

$$dx = 2 \cdot f_2 \cdot tan(\frac{\Delta\beta}{2}) \tag{20}$$

In the y-direction, the height is given by

$$y_3 = y_0 \frac{f_2}{f_1} \tag{21}$$

which is just the object height multiplied by the linear magnification.

Using these calculations and input parameters we make parameter plots showing which values of f_1, f_2 and α should be used to fully cover fill the chip in the spectral direction while still being able to fit the slit direction on the chip. One could choose the orientation of the chip (long edge in spectral direction to increase spectral resolution or long edge in slit direction to be able to fit the slit on the chip).

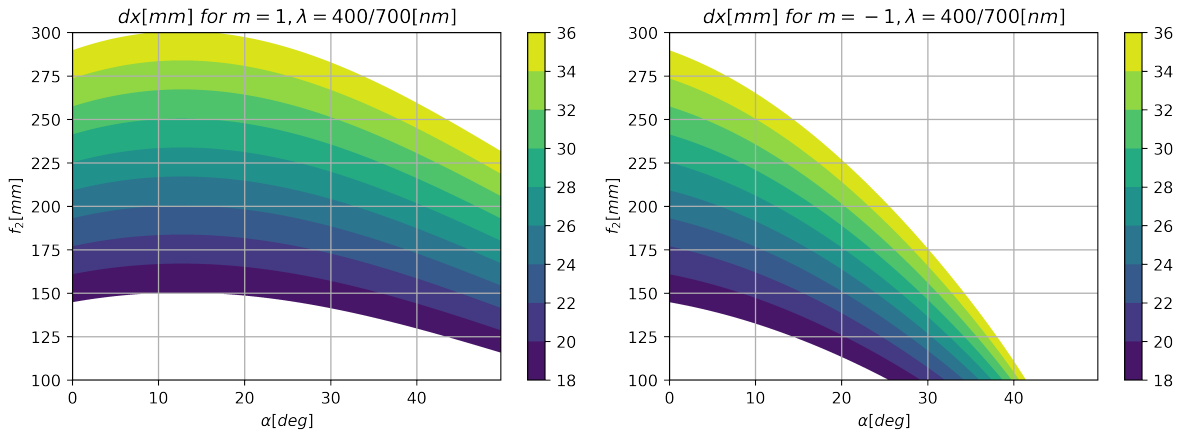

Figure 15: Figures showing the spectral width in the image plane as function of focal length of the camera lens f_2 and angle of incidence w.r.t. the grating normal α for order m= $\pm$ 1. Note that this width is independent of f_1.

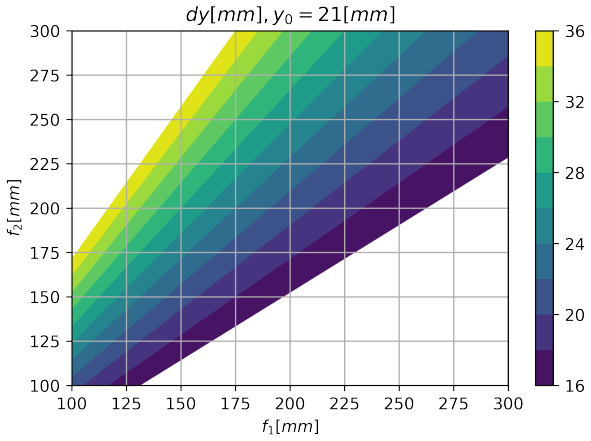

Figure 16: Figure showing the slit height in the image plane as function of focal length of collimator lens f_1 and the camera lens f_2. Note that this height is independent of α.

An example could be that we want to image the spectrum in the long edge direction of 36 [mm] and the slit in the short direction of 24 [mm]. From Figure 16 we see that we could choose f_1 to be 200 [mm] and f_2 to also be 200 [mm] so that the image height remains unchanged and is a 1-to-1 image of 21 [mm]. Now, using the given that we want to cover about 29 [mm] for the full spectrum (leaving some additional space) we find that α should be equal to about 15 [°] for m = -1.

We could also determine the minimum corresponding lens diameters of L1 and L2 based on these requirements. From the formulas as determined above and for f_1 = 200 [mm] and f_2 = 200 [mm] we find that

$$D_1 > y_1 = y_0 + 2f_1 NA_0 = 21 + 0.2f_1[mm] = 21 + 2 \cdot 200 \cdot 0.1 = 61[mm] \tag{22}$$

Since the 'object' is larger in the y-direction than in the x-direction, the first lens diameter is limited in the y-direction and should be larger than 61 [mm] to not suffer from vignetting. For the second lens, we would also like to know what the minimal lens diameter should be. For f_1 = 200 [mm] and f_2 = 200 [mm], the beam-height in the y-direction is equal to the beam-height at L1, 61 [mm]. However, due to the dispersion in the x-direction, this might actually turn out to be the limiting axis. From the

calculations above we know that the beam-width at L2 is given by

$$x_{2,t} \approx 2f_2 \cdot tan(\frac{\Delta\beta}{2}) + \frac{cos(\beta)}{cos(\alpha)} \cdot 2f_1 NA_0 \tag{23}$$

Now for $\lambda_{min} = 400\ [nm]$, $\lambda_{max} = 700\ [nm]$, d = 2.5 [$\mu$m], $\alpha = 15[^\circ]$ and in the first (m=-1) order, we find that $\beta_{min} = 24.8[^\circ]$, $\beta = \beta_c = 28.6[^\circ]$ and $\beta_{max} = 32.6[^\circ]$. Now we finally have;

$$D_2 > x_{2,t} \approx 2f_2 \cdot tan(\frac{\Delta\beta}{2}) + \frac{cos(\beta)}{cos(\alpha)} \cdot 2f_1 NA_0 = 63.7[mm] \tag{24}$$

Which is slightly larger than due required in the y-direction. Based on these calculations, we can estimate what the lens diameter of L2 should be. However, the minimum diameter is not only limited by the x- or y-direction, but rather by a combination of both since the lens is circular instead of rectangular. For this reason we estimate that the lens L2 should have a diameter of about 75 [mm], allowing for some deviations.

Now, multiple focal lengths for L1 and L2 can be found satisfying our requirements. However, if we want to image our slit in the short direction, the magnification should not exceed 1.1 making it a natural choice to set f_1 equal to f_2. Taking into account that we would like to fill our detector, and looking into commercially available lenses in combination with our grating, $f_1 = f_2 = 200\ [mm]$ is the optimal case. Based on the calculations of the minimal diameters necessary to reduce vignetting, these lenses should be faster than f/3.

4.2 Zemax/OpticStudio model

The geometrical calculations give an idea of which lenses should give the desired result. However, we would like to verify this using optical design software and implement real lenses to quantify aberrations.

4.2.1 Paraxial model

We set up a simple, paraxial model from the telescope (diameter 400 [mm] and focal length 3200 [mm] to the image plane and make a 3D figure which can be seen in Figure 17.

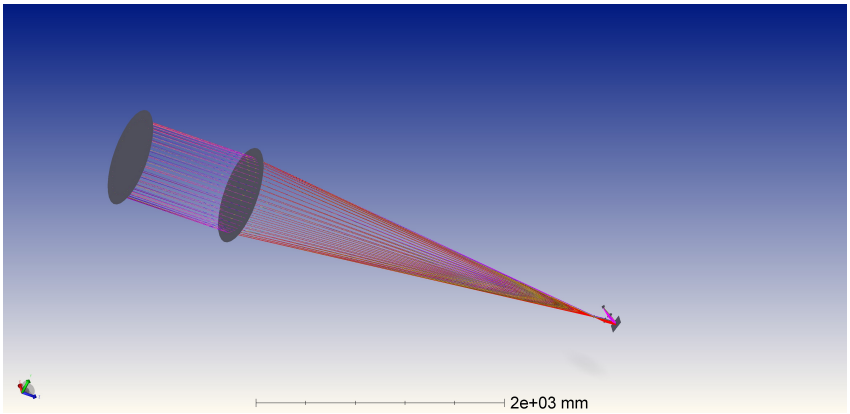

Figure 17: Image showing our paraxial model from telescope to detector.

The model does not include any parameters apart from focal lengths and diameters and the glass fibers are also not taken into account. Because of this, we made another model starting from the optical fiber output (pseudo-slit) which makes it possible to work with fiber locations instead of input angles. The 4f imaging model with f_1 = f_2 = 200 [mm] can be seen in Figure 18. We use 5 input fields at 10.5 [mm], 5.75 [mm], 0 [mm] , -5.75 [mm] and -10.5 [mm], spanning our pseudo-slit with a NA of 0.1. We use 7 wavelengths from 400 [nm] to 700 [nm] with steps of 50 [nm] and central wavelength of 550 [nm]. We set α to 15 [°] and L2 at an angle of 28.6 [°] w.r.t. the grating normal following the geometrical calculation (Zemax optimisation gives 28.4 [°]).

From this model we make a footprint plot, showing the projected locations of each wavelength and field on our detector as can be seen in Figure 19. We see our detector is indeed well filled by all fibers and all wavelengths as expected. From the data below the plot we see that the x-spread (slit direction) is equal to $2 \cdot 10.526 \approx 21[mm]$ (equal to the slit-height) and y-spread (spectral direction) is equal to $14.02 - (-13.49) \approx 27.5[mm]$ which is somewhat smaller than found from the geometrical calculations (29 [mm]). The pixel resolution is then given by

$$\frac{\Delta\lambda}{n} = \frac{300[nm]}{3000[pix]} = 0.1[nm\ pix^{-1}] \tag{25}$$

We also see that the longer wavelengths ($\sim 700[nm]$) are spread out more than the shorter wavelengths ($\sim 400[nm]$) which was also found from the geometrical calculations (grating equation). It is import to note that increasing α to relatively high angles spreads out the longer wavelengths significantly more than shorter wavelengths.

We would like to know what the spatial separation between each spectrum from one of the fibers is on our detector. From the v-groove fiber array we know that the core-to-core distance between the fibers is

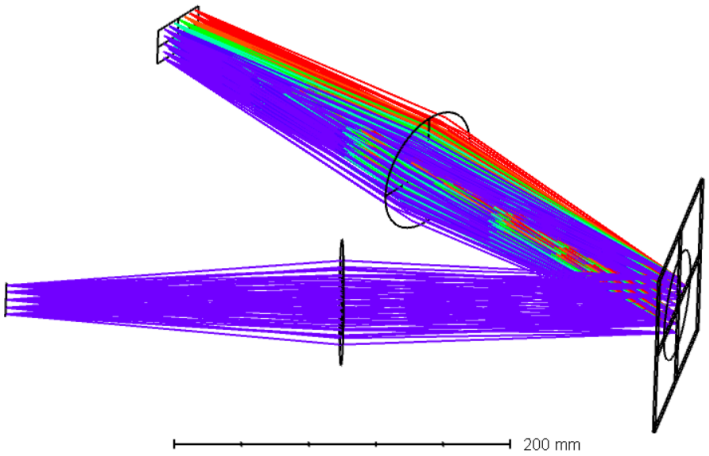

Figure 18: Image showing our paraxial model from pseudo-slit to detector. Ray-colors are corresponding with wavelengths used.

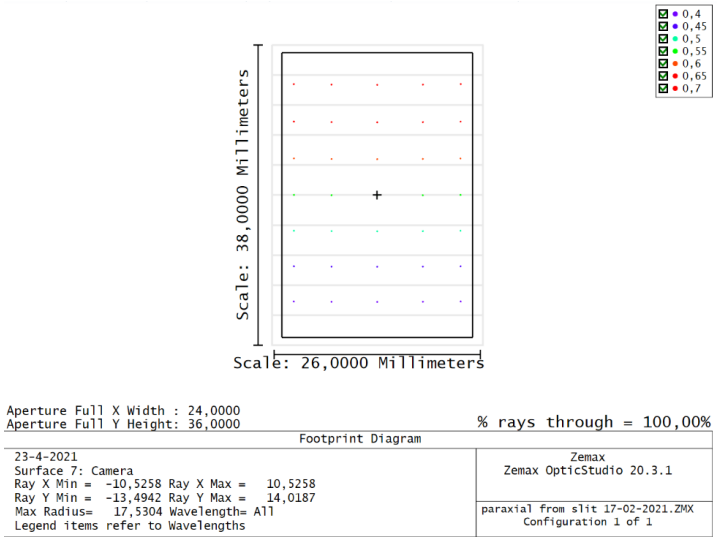

Figure 19: Image showing the footprint (image) for the paraxial model.

~ 280 $[\mu m]$ and that the core edge-to-edge distance is ~ 80 $[\mu m]$. Figure 20 shows a drawing of what the v-groove block looks like.

Two fields with $280[\mu m]$ spacing in the object plane would also correspond to $280[\mu m]$ spacing in the image plane when $f_1 = f_2$. If the spot leaving the fiber in the object plane is equal to the core-diameter of $200[\mu m]$ and our optics are perfect (paraxial), we would have an edge-to-edge separation of $80[\mu m]$ in the image-plane respectively. Since our pixels are $(9\ \mu m)^2$ this corresponds to the spectra being spaced approximately 9 pixels from each other. Of course our optics are not perfect so we don't know of it this is re-presentable. A real model should give information about if this can be reached or if we have to use more spacing so that the spectra don't significantly overlap.

4.2.2 Real model

Various lenses with focal lengths of 200 [mm] are commercially available. However not many of them have diameters larger than 70 [mm]. Furthermore, it was quickly found that spherical lenses show a lot

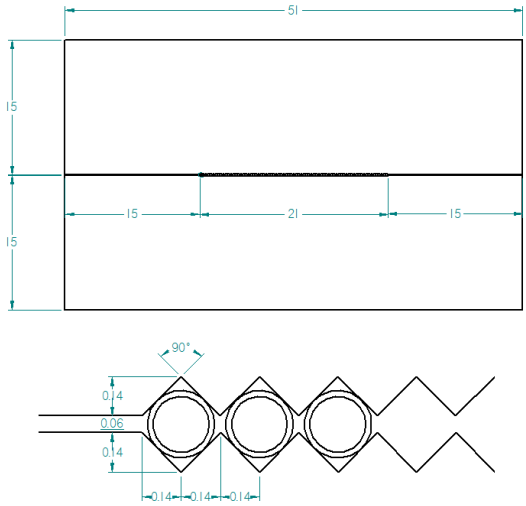

Figure 20: Drawing of the v-groove blocks holding the fibers (core and buffer visible) in the pseudo-slit with dimensions in [mm] made using Solid Edge 2020.

of spherical and chromatic aberration. Because of this, we chose to import two 200 [mm] MgF2 Coated Achromatic Lenses from Edmund Optics. These lenses can be ordered with diameters of 75 [mm], are transparent in our wavelength regime and show minimal aberration.

A model was made with the two achromatic 200 [mm] lenses which can be seen in Figure 21. α was set to 15 [°] and the system was optimised to give the smallest rms spot sizes which can be seen in Figure 22. The system can be changed such that the inner spots (fibers) have much smaller spots than the outer spots and vice versa.

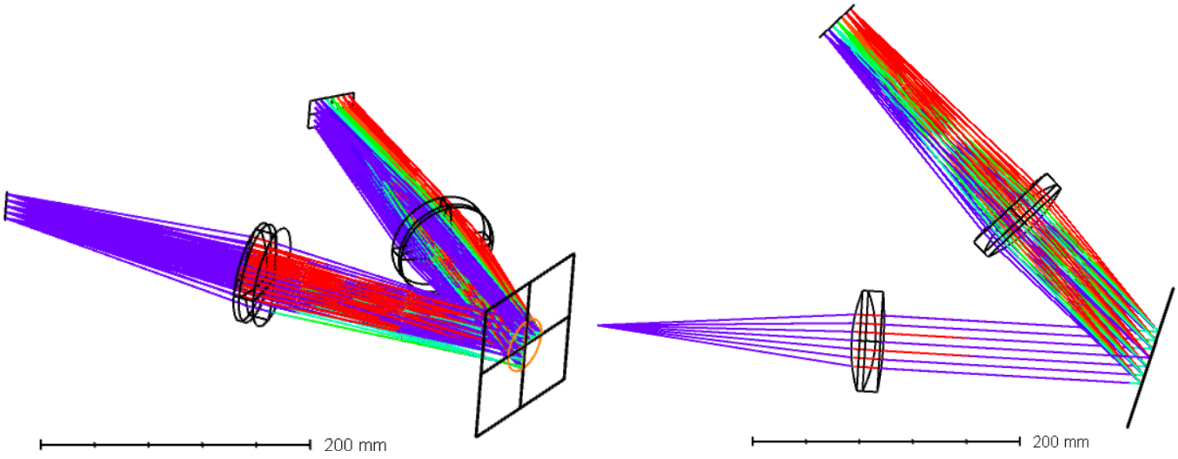

Figure 21: Figure showing the layout using the real 200 [mm] achromatic lenses.

We immediately see that the spots are quite large ($\sim 140[\mu m]$ rms) compared to the $9[\mu m^2]$ pixels. This means that 1 spot, would cover about 200-300 pixels on the detector. This is even with point sources instead of real extended ($200[\mu m]$) fiber cores so that in reality the spots would be even larger and we would see significant cross-talk between the fibers/spectra.

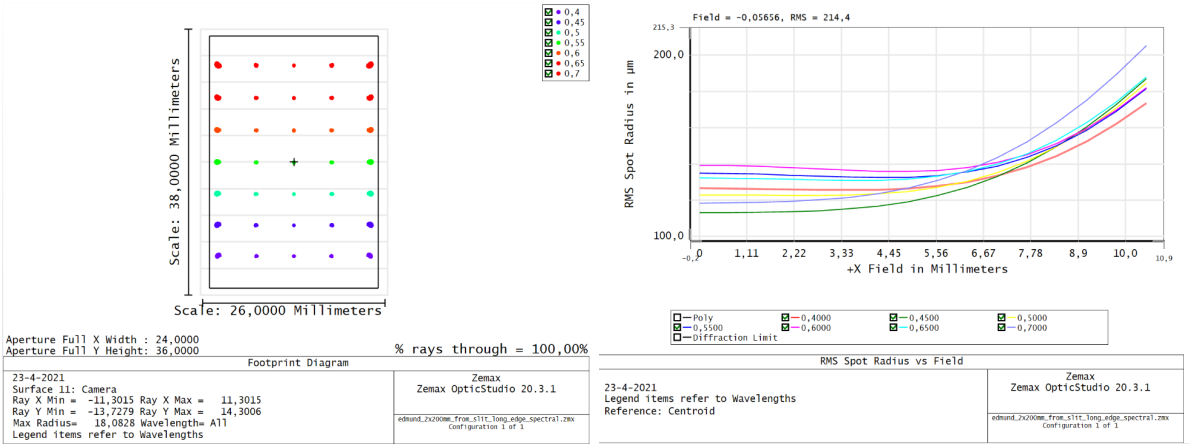

Figure 22: Left: Footprint plot using the real 200 [mm] achromatic lenses. Right: Corresponding rms spot-sizes over half the detector (dispersion direction).

Because of this is it likely not possible to separate the individual spectra using other singlet, achromatic and possibly even triplet lenses. A solution could be to increase the pitch between the fibers in the pseudo-slit. This would however also increase the total slit height, thus leading to the need of larger lenses. Another alternative might be to use high end, commercially available lenses such as photographic or projector lenses which are made to offer flat, high resolution, full-frame images. To see if photographic lenses would decrease the spot-sizes drastically enough, we implemented a standard (template) 200mm photographic lens as can be seen in Figure 23. After minimizing the x-direction rms spot sizes, the spot-figure and rms spot-sizes can in Figure 24 were found.

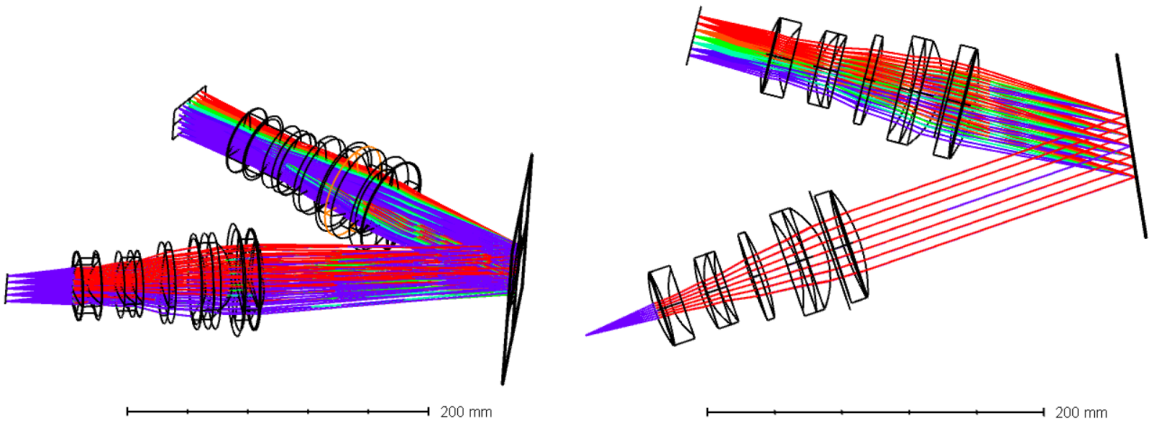

Figure 23: Figure showing the layout using 200 [mm] photographic template lenses.

Now the rms spot sizes in the x-direction are below 20 [μm] over the whole field for all wavelengths of 450 [nm] and longer. For shorter wavelengths, the rms values increase and for 400 [nm] the rms value is about 80 [μm], significantly higher. The (Real) lenses used might however perform differently than this lens in terms of optical quality or spot-sizes. Furthermore, the optical model assumes the grating to be perfect while in reality, the grating will contribute to increasing the spot-sizes. Based on the general optical performance of photographic lenses and standard pixel-sizes of DSLR cameras, it is however likely that all photographic lenses perform similarly. To substantiate this claim, Rik will perform auto-collimation tests and determine rms spot-size values over the whole full-frame field. For this reason it might be that for short wavelengths (<450 [nm]) cross-talk might become an issue. If it turns out that these short wavelengths cause problems, one might choose to include more longer wavelength to fill the

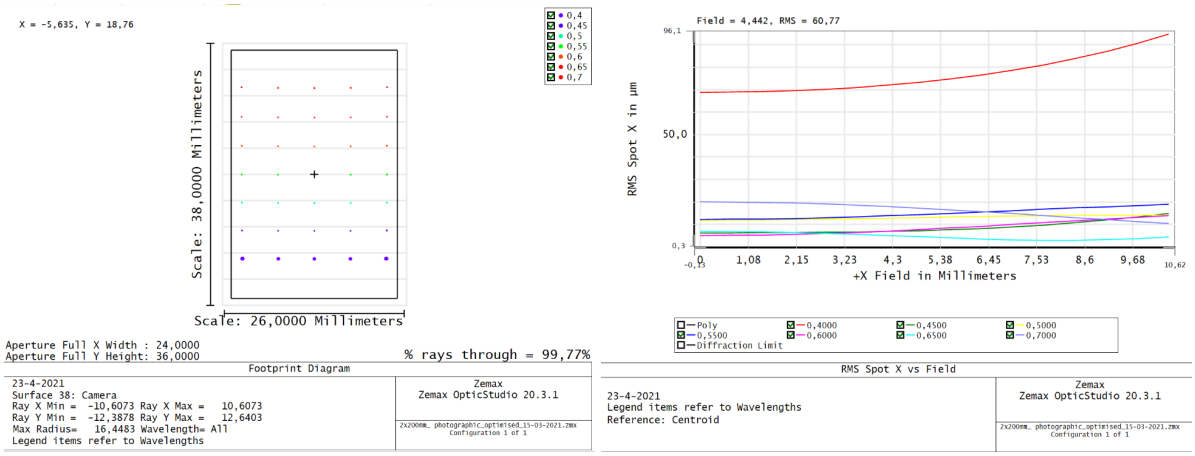

Figure 24: Left: Footprint plot using 200 [mm] photographic template lenses. Right: Corresponding rms spot-sizes over half the detector (dispersion direction).

detector. Another option is to increase dispersion by increasing α, this will fill the detector more for the same wavelength-regime, increasing the spectral resolution.

For H_α observations it might be interesting to increase the spectral resolution around 656 [nm]. For this reason we would like to find a possible configuration for wavelengths ranging from 550 [nm] to 750 [nm] spanning our detector, with 650 [nm] as primary wavelength. It was found that using the second order (m=2) of the grating with higher dispersion and using $\alpha = 0[^\circ]$ gives really good results. The layout of this (second mode) configuration can be found in Figure 25. The corresponding footprint-plot and rms spot-sizes can be found in Figure 26.

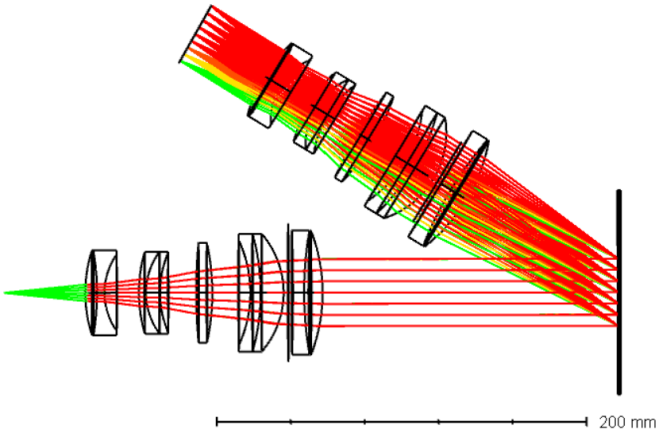

Figure 25: Figure showing the layout for higher resolution H_α observations.

From the spot-sizes we see that this set-up is almost diffraction-limited which will translate into very nice, separated spectra. Furthermore, the pixel resolution has increased to

$$\frac{\Delta\lambda}{n} = \frac{200[nm]}{3800[pix]} \approx 0.05[nm\ pix^{-1}] \tag{26}$$

The spectral resolution is however not limited by the pixels, not limited by the diffraction-limited spectral resolution of the grating but by a combination of these with fiber diameter where the latter is probably the limiting factor. It is to be experimentally determined what the final spectral resolution is.

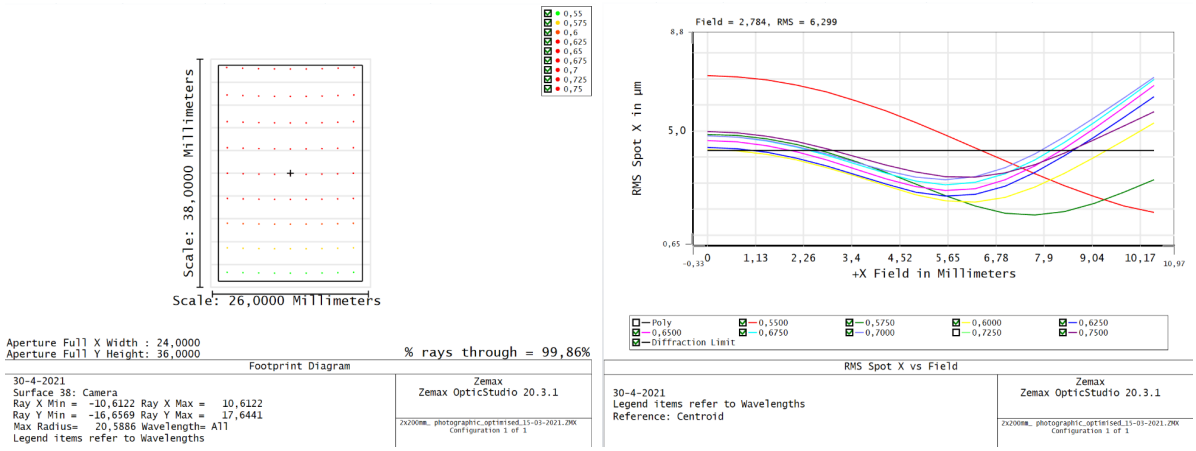

Figure 26: Left: Footprint plot for the higher resolution H_α observations. Right: Corresponding, almost diffraction-limited rms spot-sizes over half the detector.

4.3 Fiber cross-talk

Based on the estimations of the rms spotsizes from the 'typical' photographic lens as described in Section 4.2.2 we can investigate if we will be able to resolve the individual spectra and have minimal cross-talk between them. We know that in the V-groove block (Figure 20), the fiber pitch (core-to-core distance) is 280 [μm] and that the fibers have a core-diameter of 200 [μm]. We would like to estimate the cross-talk between spectra for this V-groove block to see if it will work or if we need to increase the pitch. To estimate the cross-talk between spectra, we should convolve the fiber-position dependent point spread function (PSF) with the objects spatial illumination profile (IP) and compare the projected image (spectrum) of each fiber with the adjacent fiber images.

Both of these components, the PSF and the IP are difficult to estimate without experimental testing. For this reason we will assume the PSF to be gaussian shaped (with some modifications) and use the spot rms-values obtained the photographic optical model. The IP is assumed to be uniform with some modifications. Figure 27 shows what different rms values for the gaussian PSF's and what the IP for 5 adjacent fibers with uniform illumination look like.

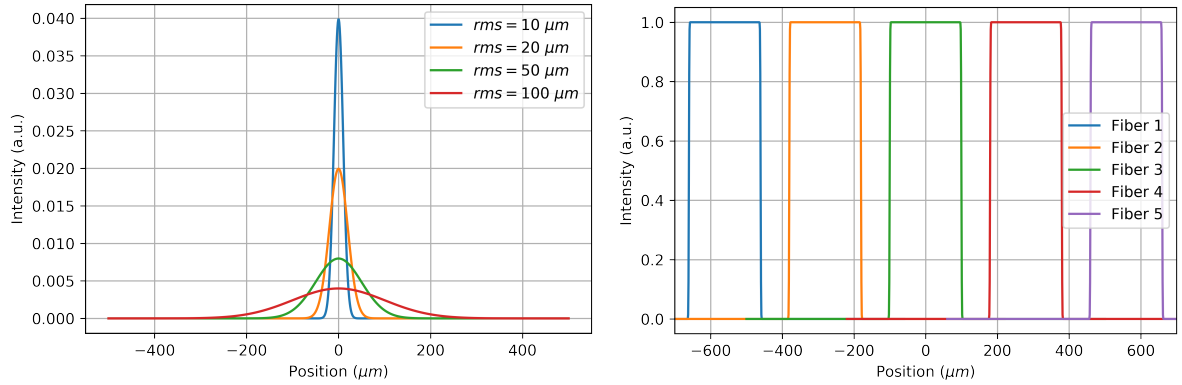

Figure 27: Left: Gaussian profiles for different rms values. For a gaussian we have that the standard deviation is equal to the rms value so that the $FWHM = 2.335\ rms$. Right: Illumination Profile for 5 adjacent (200 [μm] core and 280 [μm] pitched) fibers with uniform illumination look like.

From the IP we see that, if the illumination profile from each fiber is uniform and assuming the mag-

nification is 1-to-1 (for $f_1 = f_2$) having an significantly narrow PSF will result in a sharp cutoff and a spacing between 2 spectra of 80 [μm]. Nevertheless, the PSFs are not significantly narrow but are generally in the order of 20 [μm] as can be seen in Figure 24. Figure 28 shows what the convoluted images of the IP and PSF look like for gaussian rms values of 20 [μm] and 50 [μm] look like.

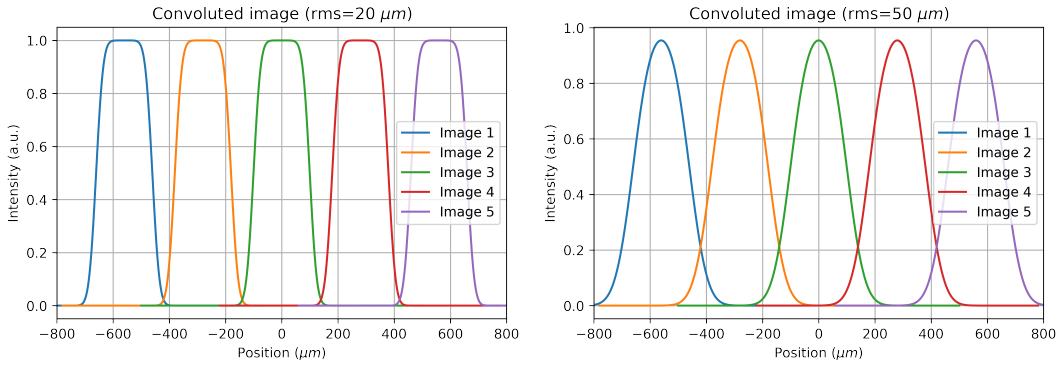

Figure 28: Left: Image of 5 adjacent fibers with uniform illumination convoluted with 20 [μm] rms Gaussian PSFs. Right: Similar to left image but convoluted with 50 [μm] rms Gaussian PSFs

We see that if the rms values are in the order of tens of microns, the images of spectra hardly overlap. Moreover, it is important to note that these calculations are 1 dimensional while in reality the fibers are 2 dimensional disks. A 2 dimensional correction for a uniform illumination (top-hat) would in fact change the illumination profile to double semi-circle, concentrating the intensity more towards the center so that the uniform illumination would give an upper bound to the overlap.

From the photographic model we obtained the spotsize rms values from which we made Gaussian PSFs. However, not all spots are Gaussian shaped. In Figure 29, two examples of typical PSF cross-sections can be seen. The left one can be well approximated by a Gaussian, while the right is better represented by two, spatially separated Gaussian's. It was found that actually many of the models PSFs are symmetric and can be represented by two Gaussian's. This does not guarantee that the spots of the system we will finally use are often of this shape but we will still check if these type of deviations might cause problems in terms of cross-talk. Instead of convolving the uniform IP with gaussians, Figure 30 and 31 show what

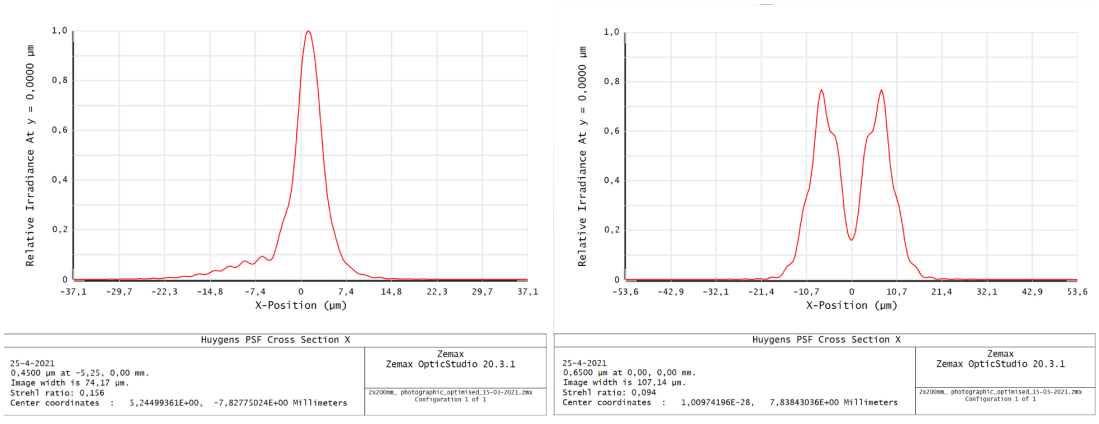

Figure 29

different (common) PSFs and their corresponding convoluted images look like.
We see that for different, common types of PSFs the corresponding spectra hardly show any overlap.

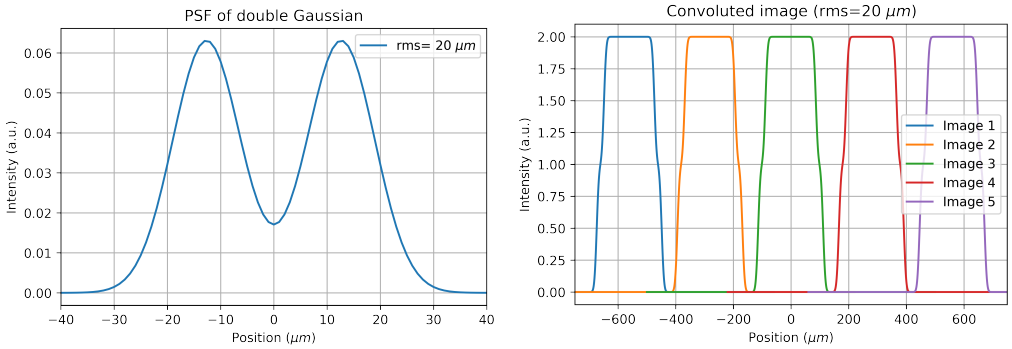

Figure 30: PSF of a double gaussian with 20 [μm] rms and corresponding convoluted image.

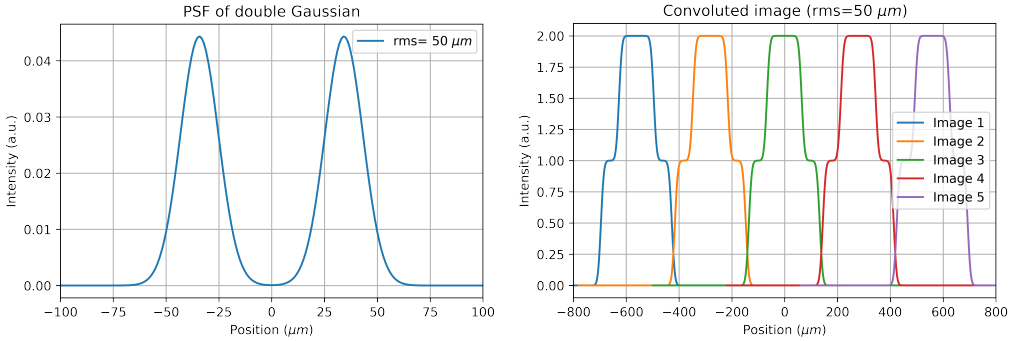

Figure 31: PSF of a double gaussian with 50 [μm] rms and corresponding convoluted image.

Even for worst-case PSFs with rms values of 50 [μm] there is no significant overlap in the images. Based on this, we don't expect that different kinds of PSFs with similar rms values will cause any issues with overlap in the spectra.
For uneven illuminated fibers (on the telescope side), the output might also be non-uniform. As stated before, Gaussian or similar IP are common. Off-axis sources might however also uneven illuminate the fiber in a way that the output (IF) might be an annulus. It would be ideal that the signal is scrambled before it enters the fiber but this is however not possible. We would like to quantify how big of a problem this such an annulus-shaped IP might be.
Using the annulus-shaped IP profile as shown in Figure 32 and the 20 [μm] single Gaussian (Figure 27) and 20 [μm] double Gaussian (Figure 30), the two corresponding convoluted images in Figure 33 were found.

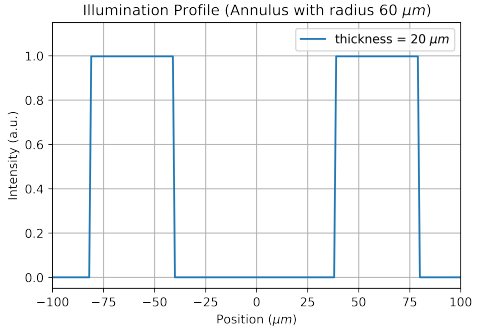

Figure 32: Annulus-shaped illumination profile with a 60 [μm] radius and 20 [μm] thickness.

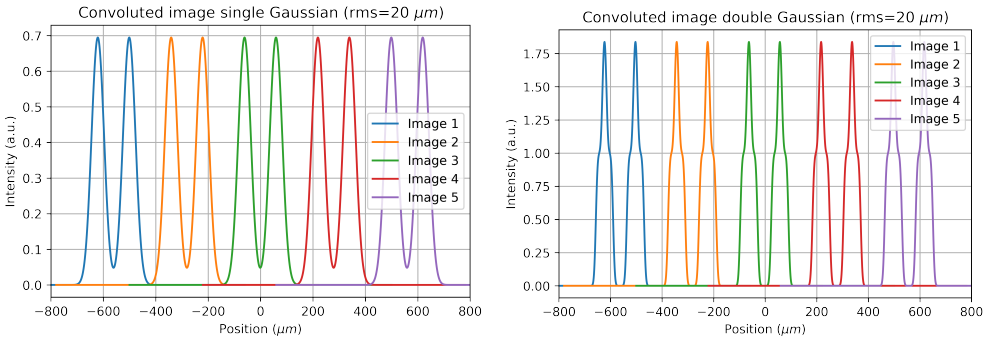

Figure 33: Convoluted images for an annulus-shaped illumination profile and single (left) and double 20 [μm] rms Gaussian (right).

From these images we see that for realstic PSFs and illumination profiles, there still is hardly any overlap in the spectra. Based on this, we can say that when rms values are in the order of tens of [μm], there will hardly be any cross-talk between fibers. Especially when keeping in mind that the illumination profile in reality is more concentrated towards the center. Only for rms values above 50 [μm], such as for the 400 [nm] wavelength, cross-talk might be a significant issue. Finally, on-chip binning might help smoothening the spectra and making the distinction between two adjacent spectra more clear and easier to work with.

5 Throughput efficiency

We would like to estimate the throughput of our system helping us determine detection limits. Assuming the system consists of 5 consecutive components (fibers, collimator lens, grating, camera lens and detector) we can just multiply the transmissions of each individual component to obtain the total transmission. The table showing the individual and total transmission for various wavelengths spanning our field op interest can be found in Table 1. Losses in the fibers can be appointed to reflection, attenuation and focal ratio degradation. The reflections are about 3.5 $\%$ at each end, attenuation is about a few $\%$ and about 20 $\%$ is due to FRD [van Assen, 2011]. The transmission of the collimator and camera lens are obtained from Figure 12, grating efficiency is obtained from Figure 11 and the detector QE is from Figure 13.

Wavelength (nm) Optical element	400	500	600	700
13m fibers	0.67	0.71	0.72	0.73
Collimator lens	0.80	0.87	0.89	0.83
Grating	0.10	0.29	0.48	0.66
Camera lens	0.80	0.87	0.89	0.83
Detector QE	0.42	0.50	0.36	0.24
Total throughput	0.02	0.08	0.10	0.08

Table 1: Approximate throughput of the spectrograph for wavelengths of interest.

6 Discussion and Conclusions

In this report we have described the optical design of the Blaauw spectrograph. Using geometric calculations and professional optical modelling software, various options of lenses and geometrical parameters are tested for suitability considering using the available optical fibers, diffraction grating and CCD detector and disregarding spectral resolution.

Using a pseudo-slit of 21 [mm] and a detector size of 24 [mm] x 36 [mm] it was found that to fill the CCD from a wavelength of 400 [nm] to 700 [nm], 2 lenses with focal lengths of 200 [mm] and an angle α of 15 [$^\circ$] gives the optimal (Low-resolution) result. Shifting the wavelength-regime from 450 [nm] to 800 [nm] is possible while going down to shorter wavelengths turned out to be difficult. For 370 [nm] the rms spot-sizes are expected to be within limits but shorter wavelengths might be unable to be resolved due to the significant spot-sizes. Another mode, using the second order of the grating, an angle α of 0 [$^\circ$] and the same lenses would cover the CCD from 550 [nm] to 750 [nm] in a higher resolution mode for H_α (656[nm]) observations. Moreover, it is possible to find similar configurations for other wavelengths of interest in higher resolution modes.

Furthermore, it was learnt that singlet and even achromatic lenses suffer from significant aberrations leading to large spots (> 140 $[\mu m]$) over the whole field causing serious cross-talk between spectra. For this reason, we decided to go for commercial off-the-shelf photographic lenses which offer a flat, high-resolution full-frame image. Since these lenses have to be fast ($\sim$ f/3), we bought 2 Canon EF 200 [mm] f/2.8 lenses for about 550 euro each which show high transmission over the full wavelength band and even into the UV. Assuming all 200 [mm] f/2.8 photographic lenses perform similarly, these lenses are expected to give spot-sizes of ~ 20 $[\mu m]$ over the whole field for wavelengths from 450 [nm] to 800 [nm] and of about 80 $[\mu m]$ for 400 [nm].

An investigation into the significance of cross-talk was done for typical rms spot-sizes and various typical spectrograph PSF's. It was found that for ~ 20 $[\mu m]$ spots, there is at maximum a few percent of overlap between spectra taking into account a fiber core diameter of 200 $[\mu m]$ and a pitch of ~ 280 $[\mu m]$. For spots of ~ 50 $[\mu m]$ there might be about 20 percent of overlap between spectra.

Finally, the total throughput of the spectrograph was estimated taking into account the available fibers, grating and detector and the bought Canon lenses. The throughput was estimated to be 0.02, 0.08, 0.10 and 0.08 for 400 [nm], 500 [nm], 600 [nm] and 700 [nm] respectively.

In this research, certain assumptions had to be made to obtain the results as given in this section. The most important factor might be that the bought 200 mm Canon lenses could not be simulated using Zemax. Due to this, similar template lenses were used which are expected to give similar results in terms of spot-sizes. This assumption is however not verified and optical bench testing of the lenses might give insight into this.

The efficiency curve of the existing grating could not be obtained and thus a typical curve was used to estimate the efficiency. Moreover, in the Zemax model, the grating is assumed to be ideal. In reality, the grating is not perfect and might influence the spots on the detector which has not been taken into account. However, following the simulated PSF's and estimated cross-talk, there is room for variation while maintaining minimal cross-talk. It was also found that our grating is not ideal for first order use with a central wavelength of 550[nm], limiting the throughput drastically. In the second order, it is fine for 550[nm] observations but limited by the free spectral range and thus not suitable for low-resolution 400 [nm] to 700 [nm] observations.

Since this report only proposes a theoretically functional design for the spectrograph, we cannot say that it works as expected when built. Before First-light commissioning or even setting everything up, some tests have to be done to give insight into its (provisional) functioning. The next step which has to be taken is to make a setup for testing the bought lenses for vignetting and induced spot-sizes. To do this, the lens-mounts and camera-connector have to be built first. If the spots turn out to be reasonable (< 20 $[\mu m]$) over the whole 24 [mm] x 36 [mm] field, they are validated and are expected to work properly for the spectrograph. Next, when the grating-mount is built, we can make the full set-up using the CCD, grating and both lenses. Testing will tell us if the spectrograph works as expected and how much tip/tilt tweaking or other optical alignment of the grating, lenses and possibly CCD or pseudo-slit is necessary. A full efficiency curve of the grating would be helpful. Using one single optical fiber with variable height (micrometer positioning) and the available spectral-lamps as input will give an estimate to the spot-sizes over the whole field as projected by the fiber and will tell us the expected cross-talk between spectra. This test will also clarify the achievable spectral resolution for the combined setup. If the cross-talk behaves as expected, the pseudo-slit and IFU-head can be built and both ends can be polished and placed as planned. Back-illumination tests have to be done and a suitable method has to be implemented for quick but accurate calibration. The full spectrograph can then have its first light to determine its performance.

After the spectrograph is commissioned, possible improvements are buying a 50 [mm] x 50 [mm], 600 [l/mm], 500 [nm] blazed grating to increase efficiency in the wavelength-regime of interest. Furthermore, a robotic rotator for the grating and possibly a separately rotating arm for the CCD camera and camera lens could be bought to allow for smooth transitions between high- and low resolution modes without having to re-align and test the optical layout. A data-pipeline could be programmed to do background subtraction and extract all the 75 spectra from one image based on pixel-positions and relate all spectra to their corresponding position on the sky (based on the labelled fibers) to obtain data-cubes.

7 Appendix

7.1 List of the component's critical parameters

Primary mirror diameter	400 [mm]
Focal length	3200 [mm]
plate scale	64.5 [arcsec mm^{-1}]

Table 2: Table showing critical parameters of the Gratama telescope.

Number of fibers used	61 science- /12 sky- / 2 spare- fibers (75 total)
Fiber diameter core/clad/buffer	200/220/240 [μm]
Fibers length	$\sim$ 13 [m]
Output $f/\#$ (f/8 in)	f/5 (80 $\%$ integrated light)
Single fiber sky projection	$\sim$ 12.9 [arcsec]

Table 3: Table showing critical parameters of optical fibers used.

Focal length	200 [mm]
f/#	f/2.8
Back focal length	44 [mm]
Size (DxL)	83 [mm] x 144 [mm]
Weight	810 [g]

Table 4: Table showing critical parameters of collimator- and camera lens used.

Size (width x height)	110 [mm] x 110 [mm]
Line spacing	2.5 [μm] (400[l/mm])
Blaze angle	9.773 [$^\circ$]

Table 5: Table showing critical parameters of diffraction grating used.

Chip Size	36.0 [mm] x 24.7 [mm]
# Pixels	4008 x 2672)
pixel size	9 [μm] x 9 [μm]

Table 6: Table showing critical parameters of detector used.

7.2 Low resolution configuration

A schematic overview of the optical layout can be found in Figure 34. This layout shows the low-resolution configuration with full spectral coverage from 400 [nm] to 700 [nm], angle of incidence 25 [deg] and using order m =-1. The distances are in [mm] (physical lens length $\sim$ 144 [mm] and back focal distance $\sim$ 44 [mm]). The distance L2+L3 can be varied to minimize throughput and back-scattering from adjacent orders (m=0 gives 50 [°] and m=-2 gives $\sim$ 30 [°] @ 400 [nm]). The aperture stop will also be inside L2+L3, which can be used to minimize order cross-talk or aberrations on the edges of lens 2 but will also limit the grating resolution. Making L2+L3 smaller will result in a smaller input cone for lens 2, but a physical limit is set due to the size of the lenses.

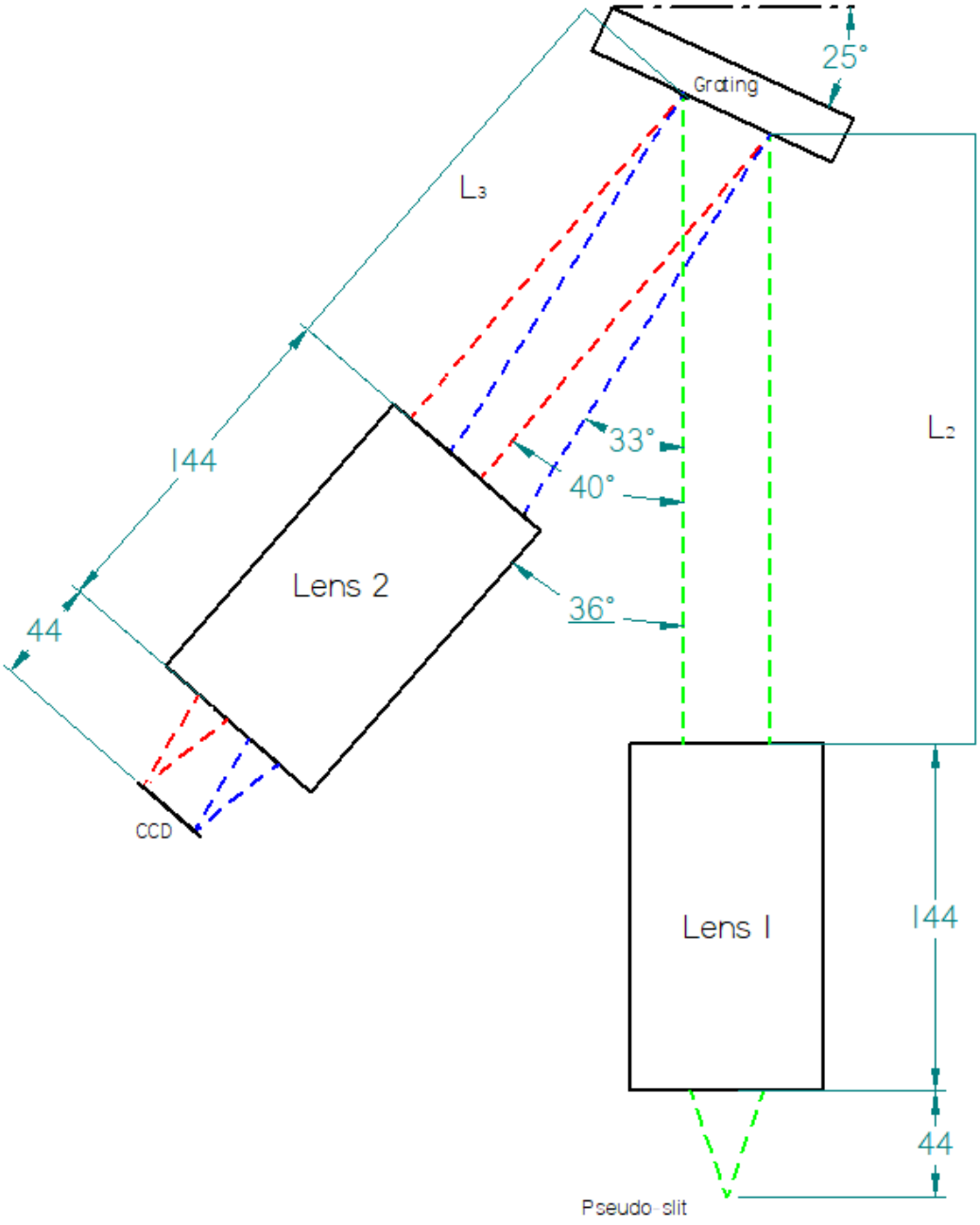

Figure 34: Figure showing a possible LR (m=-1) configuration.

8 References

[CAOS, 2021] CAOS (2021). Measuring transmission for canon objectives. https://spectroscopy.wordpress.com/2011/03/27/measuring-transmission-for-canon-ef-200mm-f2-8l-ii/.

[Diffraction-limited, 2021] Diffraction-limited (2021). Stxl-11002. https://diffractionlimited.com/product/stxl-11002m/.

[van Assen, 2011] van Assen, V. (2011). Focal ratio degradation in optical fibres. Internal document.